IEEE Access
Multidisciplinary | Rapid Review | Open Access Journal

Received November 19, 2019, accepted December 10, 2019, date of publication December 19, 2019,
date of current version December 31, 2019.

Digital Object Identifier 10.1109/ACCESS.2019.2960885

Differentially-Fed, Wideband Dual-Polarized Filtering Antenna With Novel Feeding Structure for 5G Sub-6 GHz Base Station Applications

YAPENG LI, ZHIPENG ZHAO, ZHAOYANG TANG, AND YINGZENG YIN
National Key Laboratory of Antennas and Microwave Technology, Xidian University, Xi'an 710071, China
Corresponding author: Yingzeng Yin (yyzeng@mail.xidian.edu.cn)

ABSTRACT In this paper, a differentially fed, wideband dual-polarized patch antenna with filtering response is proposed. A novel E-shaped feeding structure with one end shorted to the ground is proposed to excite a square patch antenna, and an extra resonant mode is induced, which leads to a wider operation band. Besides, symmetric open/short-circuited stepped impedance resonators (O/SCSIRs) are proposed to generate the third resonant mode. And the bandwidth is further improved. Moreover, the gain-suppression level outside the operation bands is greatly enhanced as the introduction of O/SCSIRs. A prototype of the proposed antenna is fabricated and tested. Measured results show that the proposed antenna has a wide operation band of 22.2% (3.12–3.9 GHz) for active VSWR < 1.5. Stable in-band gains of 8.1 ± 0.3 dBi and unidirectional radiation patterns are also obtained. Moreover, the out-of-band gain suppression level is better than 18.5 dB. A 1×4 liner array is also developed to validate our design. Good radiating performance of the proposed antenna makes it a promising candidate for 5G Sub-6 GHz base station applications.

INDEX TERMS Base station antenna, differential antenna, filtering antenna, wideband antenna, 5G Sub-6 GHz application.

I. INTRODUCTION

With the explosive development of wireless communication industry in recent years, more challenges are put forward for base station antennas in the fifth generation (5G) communication systems, such as more compact sizes, wider operation bands, lower profiles, lower costs, as well as higher selectivity.

In base station antenna systems, wideband dual-polarized antennas are widely used to increase the channel capacity. To enhance the impedance bandwidth of dual-polarized antennas, various methods are applied, such as using folded dipoles with shorting stubs [1], loading parasitic structures [2]–[4], using feeding structures of different resonant modes [5] and shifting different resonant modes together with shorting pins and slots [6]. Meanwhile, as the operating frequency of 5G base station antennas are mostly higher than 2/3/4G, the manufacturing accuracy makes it a trend for antennas to have simpler structures, easier to be fabricated, as well as lower profiles. Besides, as various antennas are integrated together to achieve multiple functions, the electromagnetic environments get worse, which makes it an urgent demand for interfere-suppression. Thus, antennas with filtering responses are highly demanded for base station antennas. In filtering antenna designs, filtering structures are largely integrated with antennas to get high out-band gain-suppression levels [7]–[11]. Although this may introduce some insertion loss, good filtering responses can also be obtained. For example, dual-mode stub-loaded resonators are proposed in [7] to excite two radiating patches, and excellent filtering response of the realized gain is generated. In [10], filtering baluns are integrated into the feedline, and a dual-polarized dielectric resonator antenna with good high selectivity is designed. In recent years, some other filtering antennas with less filtering structures or without filtering structures are also proposed for simplify designs [12]–[20]. For example, in [12], by etching open slots on a square radiating patch, radiating nulls are observed outside the operation band. The antenna has a simple structure and the two radiation nulls can be individually tuned by changing lengths of the slots. In [15], two orthogonal H-shaped feed lines are proposed to excite the driven patch, and a

The associate editor coordinating the review of this manuscript and approving it for publication was Andrei Muller.

radiation null is observed at lower band. With a stacked patch added, an additional radiation null is generated at upper band. In [16], different parasitic patches are introduced in a rectangle radiating patch, by changing the electric and magnetic coupling characteristics of the two parasitic patches, two radiation nulls are achieved. In [17] and [18], simple open stubs are proposed to excite dielectric resonator antennas with good bandpass filtering responses. In [19], a ring slot and a series of shorting vias are introduced into a triangular patch, and a quasi-elliptic bandpass response is obtained.

However, in most of the dual-polarized antenna designs, especially for base station antenna designs, wide operation band with stable radiating performances, compact sizes and high selectivity should all be taken into consideration. In view of this, a differentially-fed, dual-polarized antenna with wide operation band and good filtering response is proposed in this paper. A novel E-shaped feeding structure is introduced to excite the square radiating patch. With one end of it shorted to the ground, an extra resonant mode is observed. Besides, with four open/short-circuited stepped impedance resonators (O/SCSIRs) integrated into the feedlines, a good bandpass filtering response is achieved, as well as an additional resonant mode and a better impedance matching performance. Both the antenna element and 1×4 liner array is fabricated and tested to validate our design. The detailed design process and measurement results are discussed in the following sections.

II. ANTENNA DESIGN AND ANALYSIS

A. ANTENNA GEOMETRY

Fig. 1 illustrates the configuration of the proposed wideband dual-polarized filtering antenna. The antenna consists of two layers. The upper layer is a F4B substrate with the dielectric permittivity of 2.65, and thickness of 0.5 mm. The radiating patch and E-shaped feeding structure are printed on the top layer of the upper substrate. One end of each E-shaped feeding structure is shorted to the ground with metal posts. The lower layer is a F4B substrate with the dielectric permittivity of 2.65, and thickness of 0.8 mm. Besides, four pairs of O/SCSIRs are printed on the top layer of the lower substrate. The four ends that close to the center of the substrate are connected to the E-shaped feeding structures with metal posts. The other four ends of the O/SCSIRs are connected with 50 Ω coaxial cables. A metal ground is printed at the bottom layer of the lower substrate with four U-shaped slots. When port1 and port2 are excited with differential signals, a $+45°$ polarization is generated. Similarly, a $-45°$ polarization can be obtained when port3 and port4 are excited with differential signals. As the proposed antenna is totally symmetric about the center point, the two polarizations have similar port characteristics and radiation performance. Thus only the performance of the $+45°$ polarization is displayed for brief demonstration.

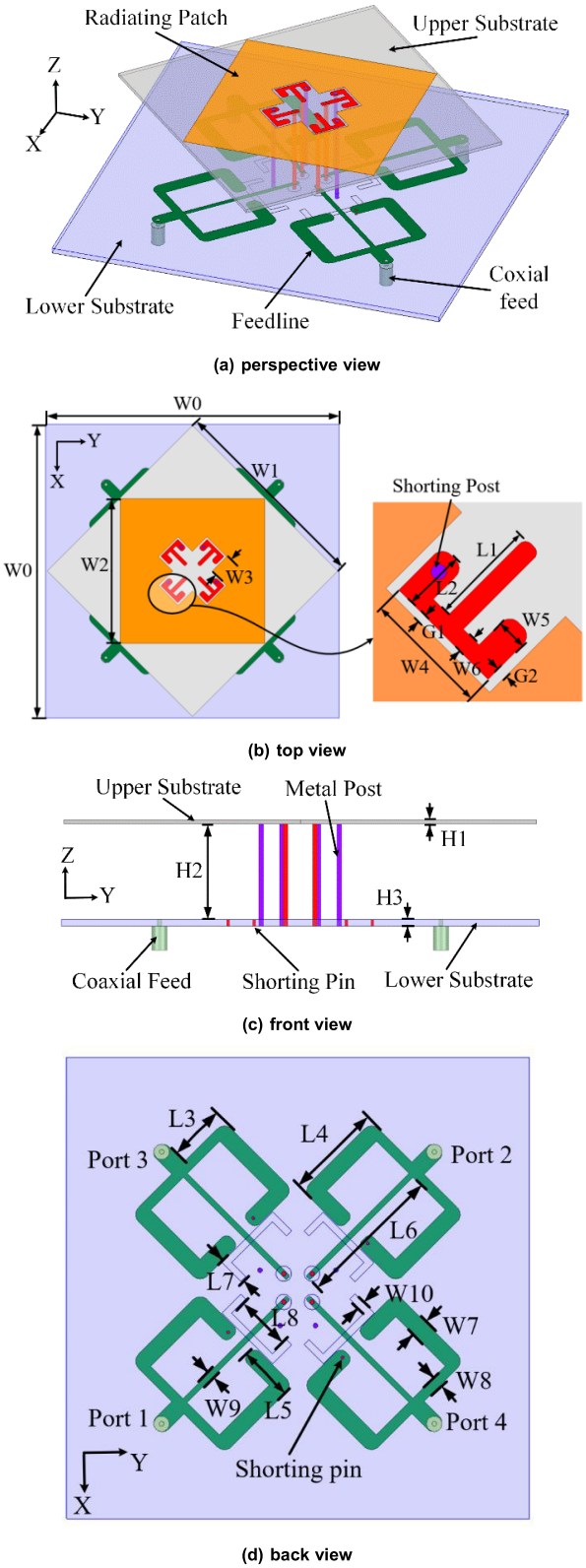

FIGURE 1. Configuration of the proposed antenna: (a) 3-D view, (b) top view, (c) front view and (d) top view of the lower substrate. The optimized parameters are as follows (unit: mm): W0=65, W1=42, W2=0.1, W3=1.0, W4=2.1, W5=1.1, W6=0.2, W7=1.6, L1=27.2, L2=4.6, L3=10.3, L4=13.4, L5=6.5, L6=8.0, L7=3.2, L8=10.3, L9=14 0, Ls=25.0, H1=0.8, H2=0.5, H3=10.0.

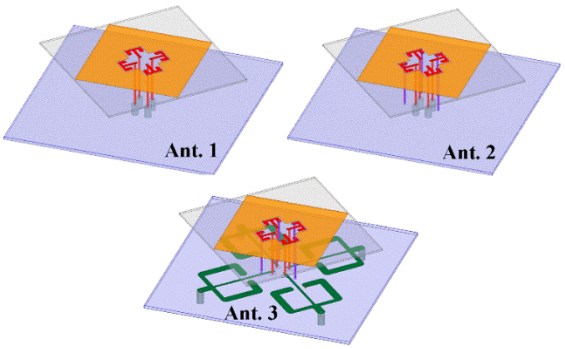

FIGURE 2. Evolution process of the proposed wideband patch antenna.

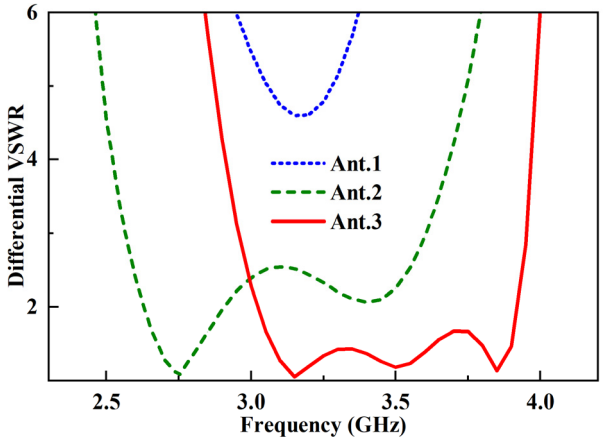

FIGURE 3. Simulated differential VSWR for the three antennas.

B. BANDWIDTH ENHANCEMENT OF THE PATCH ANTENNA

To explain the operation principal of the proposed antenna, an evolution process for bandwidth enhancement of the patch antenna is shown in Fig. 2. The corresponding differential VSWRs for the antennas are plotted in Fig. 3. The conventional differentially-fed dual-polarized patch antenna (Ant.1) consists of a square radiating patch, four E-shaped feedlines and four metal posts which are connected with 50-Ω coaxial cables. Simulated results show that Ant.1 has a single operating band at about 3.18 GHz. Ant.2 is four shorting pins added to ends of the E-shaped coupling structures. It can be seen that the first resonant mode moves to lower band (at about 2.73 GHz), and another resonant mode occurs at about 3.42 GHz with improved impedance matching performance. Ant.3 is four symmetric open/short-circuited stepped impedance resonators (O/SCSIRs) added to Ant. 2. The O/SCSIRs are printed on the top layer of the lower substrate with the four metal posts connected to the ends. And the other four ends are connected to coaxial feeds. It can be seen clearly from Fig. 3 that the first resonant mode is moved back to about 3.15 GHz. Besides, the O/SCSIRs provide another resonant mode at about 3.95 GHz with better impedance matching performance.

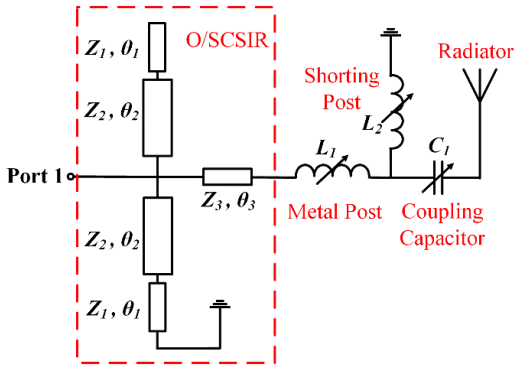

FIGURE 4. Equivalent circuit of Ant.3 from port 1 to the radiator.

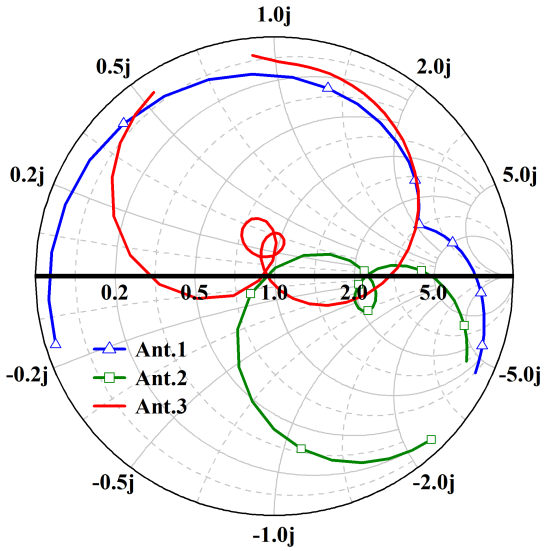

FIGURE 5. Simulated active input impedance in Smith chart.

For better demonstration of the resonant characteristics, the equivalent circuit from one port to the radiator and the active input impedance for the antennas are illustrated in Fig. 4 and Fig. 5, respectively. As the properties of feeding structures change with frequency, the inductances/capacitors for the equivalent circuit are set as variables. It can be seen that the resonant characteristics of Ant.1 is determined by the metal post (L1), the coupling capacitor (C1) and properties of the radiator. Thus, two resonant modes should be observed for Ant.1. One is produced by L1 and C1, the other is produced by the radiator. While, the two resonant modes are too close and merge into one, which can be seen clearly in Fig. 5. When the shorting posts are introduced (the parallel inductance L2 is added), the overall inductance decreases, and the first resonant mode moves to lower frequencies. Thus, the two resonant modes are separated by the shorting posts, and a wide operation band is obtained for Ant.2, which can also be observed from Fig. 5. As the O/SCSIR is printed on the lower substrate of Ant.3, the ABCD matrix and S-parameter of the equivalent circuit for it can be calculated as follows:

$$\begin{bmatrix} A & B \\ C & D \end{bmatrix} = \begin{bmatrix} 1 & 0 \\ Y & 1 \end{bmatrix} \begin{bmatrix} \cos\theta_3 & jZ_3 \cdot \sin\theta_3 \\ j\sin\theta_3/Z_3 & \cos\theta_3 \end{bmatrix} \quad (1)$$

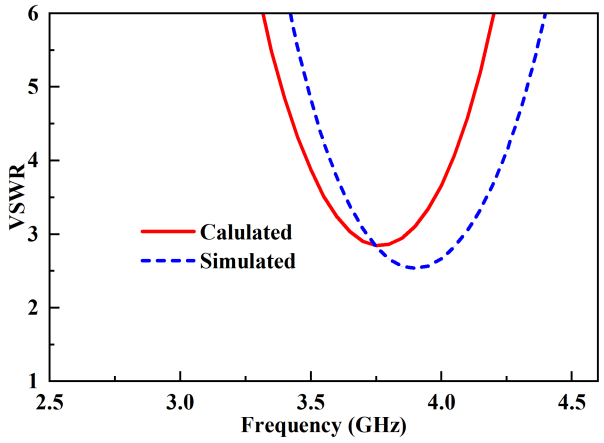

FIGURE 6. The simulated and calculated VSWR for the O/SCSIR.

$$Y = \frac{j}{Z_2} \cdot \left(\frac{Z_2 + Z_1 \cdot \cot\theta_1 \cdot \tan\theta_2}{Z_1 \cdot \cot\theta_1 - Z_2 \cdot \tan\theta_2} - \frac{Z_2 - Z_1 \cdot \tan\theta_1 \cdot \tan\theta_2}{Z_1 \cdot \tan\theta_1 + Z_2 \cdot \tan\theta_2} \right) \quad (2)$$

$$S_{11} = \frac{A + B/Z_0 - C \cdot Z_0 - D}{A + B/Z_0 + C \cdot Z_0 + D} \quad (3)$$

The calculated and simulated VSWRs are illustrated in Fig. 6. It can be seen that the O/SCSIR provide an additional resonate mode at higher frequency band. When it is introduced into the feedline of Ant.3, a wide operation band with three resonant modes are obtained.

Some parameters are studied to investigate the influence of the feedline on the bandwidth of Ant.3. Fig. 7 shows the resonant characteristics change with L2. As illustrated in Fig. 4, the overall length of the shorting part (L1+L2+0.5*W4+H2+H3) gets longer as L2 increases, and the inductance is enhanced. Meanwhile, the whole equivalent circuit is capacitive at higher band. As a result, the impedance matching performance gets better at higher frequencies. Fig. 8 shows the resonant characteristics change with W4. It can be seen that the first and third resonant mode move to lower frequencies, with the second one moves to higher band. As the radiator is coupled by the E-shaped feeding structure, the coupling capacitor C1 strengthens when W4 increases, and the overall inductance is furtherly suppressed. Thus, the first and third resonant mode move to lower band. However, length of the shorting pin is also enlarged, and inductance of the shorting pin increases at the same time. As a result, the second resonant mode move towards upper band.

C. FILTERING RESPONSE OF THE PROPOSED ANTENNA

The realized gains of the antennas in the last section and the final design (four U-shaped slots added to Ant.3) are illustrated in Fig. 9. It can be seen that the O/SCSIRs can provide high selectivity for the patch antenna except for bandwidth-enhancement performance. Two radiation nulls are observed outside the operation band for Ant.3 with sharp roll-off. The transfer characteristic for the O/SCSIR can be calculated as

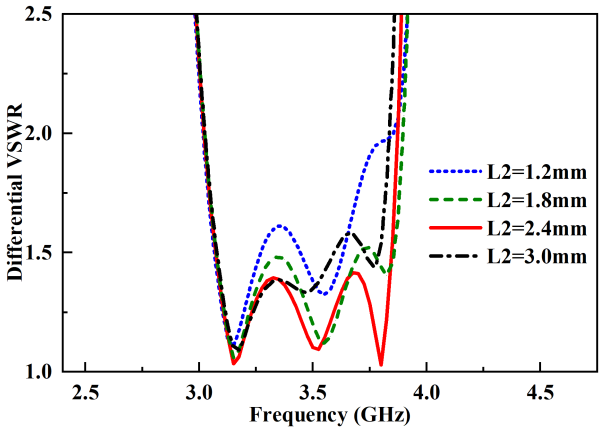

FIGURE 7. Simulated differential VSWR of Ant.3 change with L2.

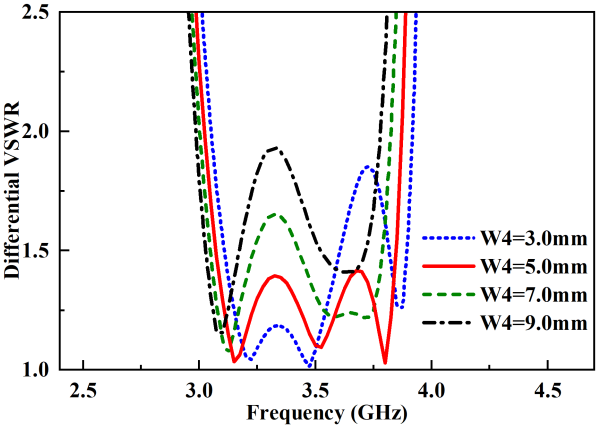

FIGURE 8. Simulated differential VSWR of Ant.3 change with W4.

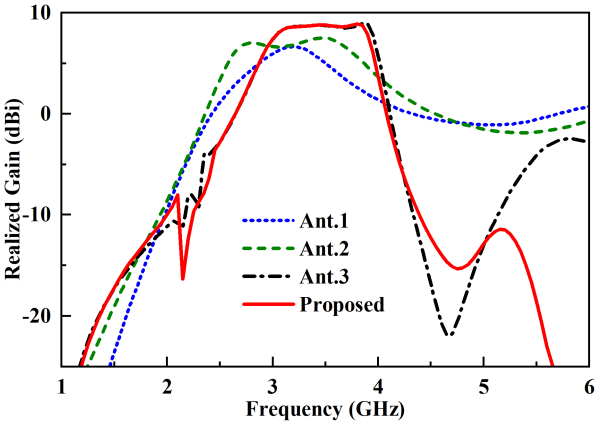

FIGURE 9. Simulated realized gains for the antennas.

follows:

$$S_{21} = \frac{2}{A + B/Z_0 + C \cdot Z_0 + D} \quad (4)$$

Here, values for A, B, C and D can be get from equation (1) and (2). Frequencies of the radiation nulls can be obtained when transmission zero occurs, which means S21=0. As the

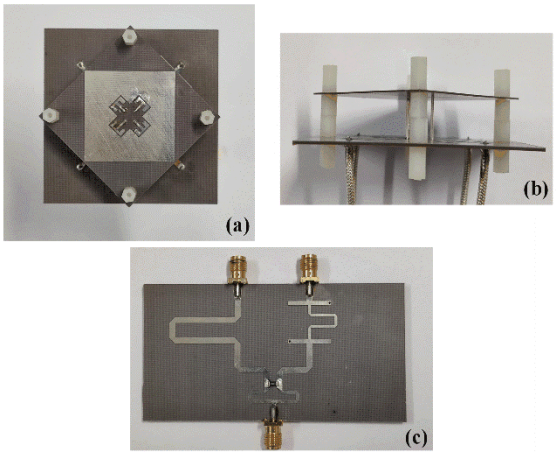

FIGURE 10. Prototype of the proposed antenna: (a) top view, (b) side view and (c) 180° hybrid coupler.

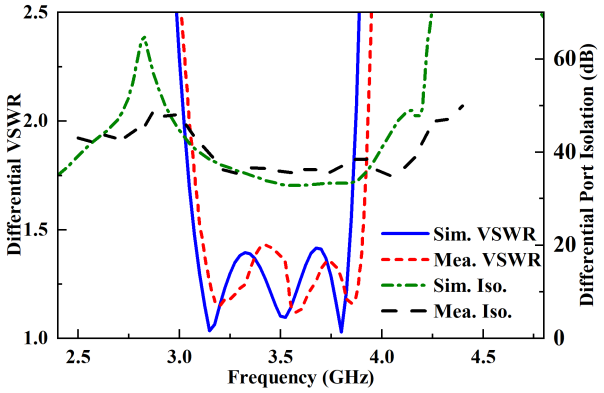

FIGURE 11. Simulated and measured differential VSWR and differential port isolation of the proposed antenna.

microstrip line with length of $\theta 3$ is designed for impedance matching, the equation can be simplified to Y=0. And then, the transmission zeros can be calculated when equation (5) is satisfied:

$$K^2 + \frac{1}{2}\left(\frac{\tan\theta_1}{\tan\theta_2} + \frac{\tan\theta_2}{\tan\theta_1} - \frac{1}{\tan\theta_1 \cdot \tan\theta_2} - \tan\theta_1 \cdot \tan\theta_2\right) \cdot K + 1 = 0 \quad (5)$$

where K is the ratio of Z2 to Z1. By properly choosing length and width of the O/SCSIR, two transmission zeros can be obtained, which correspond to the two radiation nulls. To get a better gain-suppression performance, four U-shaped slots are etched on the ground plane. And the realized gain at the higher band is well suppressed.

III. EXPERIMENTAL RESULTS WITH ARRAY APPLICATION

To validate our design, a prototype of the proposed antenna is fabricated and measured, as shown in Fig. 10. A four-port R&S ZNB20 Vector Network Analyzer is used to measure the differential VSWR and differential port isolation of the antenna. Besides, a SATIMO multi-probe spherical near-field system is used to measure the realized gain, as well as the radiation patterns, and two 180° hybrid couplers are connected to each pair of differential ports in measurement process.

Fig. 11 shows the simulated and measured active VSWRs and differential port isolations for the proposed antenna.

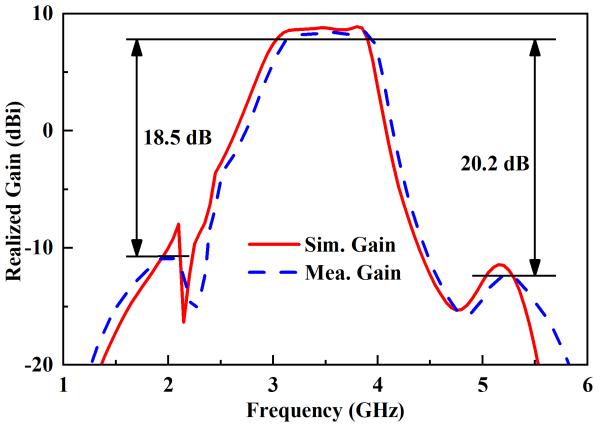

FIGURE 12. Simulated and measured realized gains of the proposed antenna.

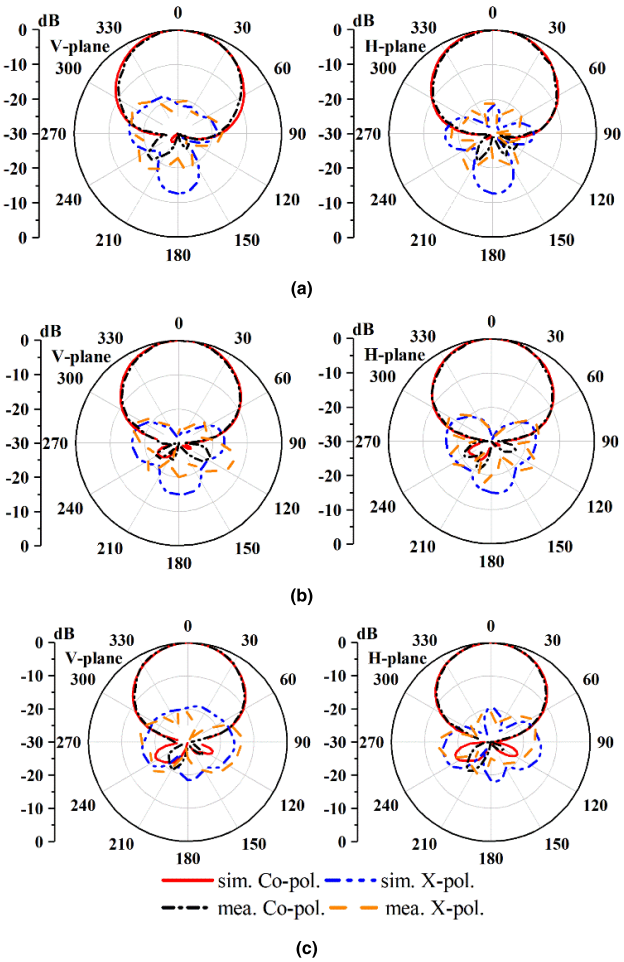

FIGURE 13. Simulated and measured radiation patterns of the antenna element at (a) 3.2 GHz, (b) 3.5 GHz and (c) 3.8 GHz.

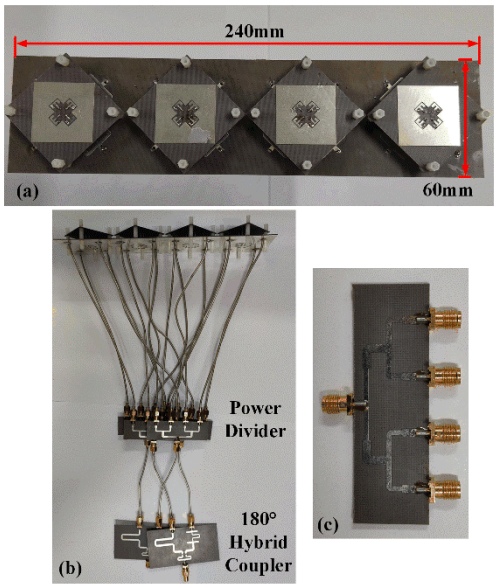

FIGURE 14. Configuration of the 1×4 antenna array: (a) top view, (b) side view. (c) power divider.

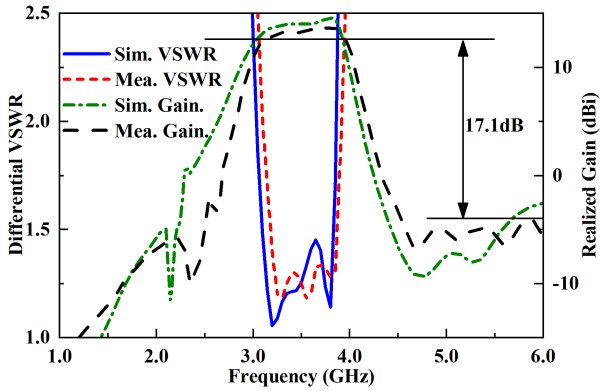

FIGURE 15. Simulated and measured differential VSWR and realized gain of the antenna array.

Measured results show that the antenna has a wide operation band from 3.12 GHz to 3.9 GHz for active VSWR<1.5. Three resonant modes can be observed significantly. Besides, the measured in-band isolation between the two polarizations is better than 35.2 dB. Fig. 12 shows the measured realized gain for the proposed antenna. It can be observed that the antenna has a flat in-band gain of 8.1 ± 0.3 dBi. Two radiation nulls can be seen obviously at 2.25 GHz and 3.85 GHz. Besides, the out-band gain suppression level is better than 18.5 dB and 20.2 dB outside the sideband, separately. Besides, measured results show that the antenna has a stable HPBW of 64° ± 4°, which is in good agreement with the simulated ones. The measured and simulated radiation patterns for the antenna element at 3.2 GHz, 3.5 GHz and 3.8 GHz are displayed in Fig. 13. Stable and unidirectional radiation patterns with low cross-polarization levels of better than −21 dB can be observed across the desired band.

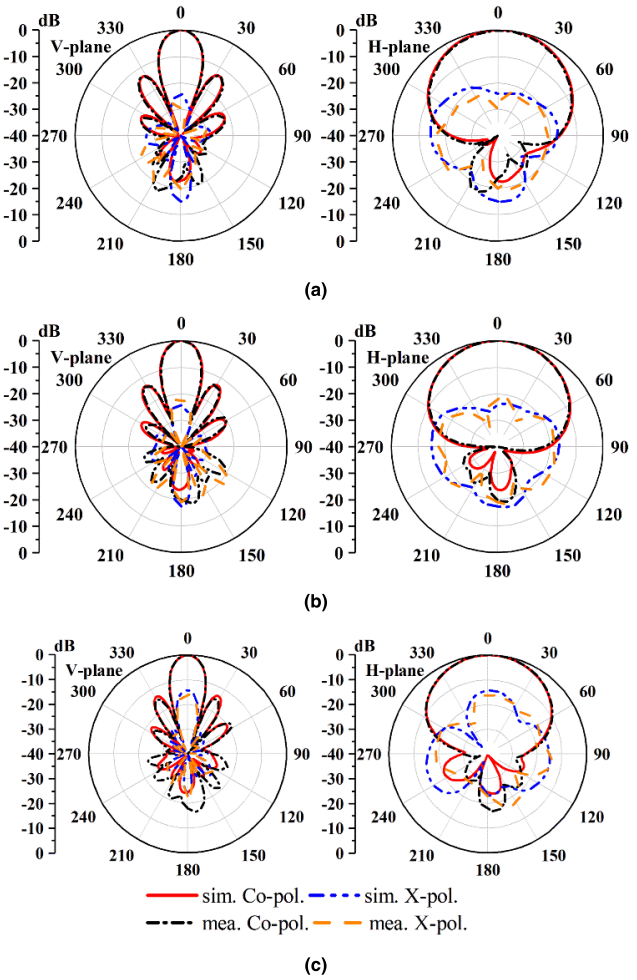

FIGURE 16. Simulated and measured radiation patterns of the antenna array at (a) 3.2 GHz, (b) 3.5 GHz and (c) 3.8 GHz.

A four-element liner array is also designed to meet the demand for 5 G Sub-6 GHz base station applications, which is shown in Fig. 14. The scheme diagram for the antenna array of our design is the same with [1]. The space between element centers is 60 mm, which is 0.7 wavelength at 3.5 GHz. Simulated and measured active VSWRs and realized gains are displayed in Fig. 15. It can be seen that the antenna array has a wide operation band from 3.18 GHz to 3.85 GHz for active VSWR<1.5. The measured in-band gain is 13.4 ± 0.5 dBi. Besides, the out-band gain suppression level is better than 17.1 dB, which indicates a good bandpass filtering response. Fig. 16 shows the simulated and measured radiation patterns of the antenna array at 3.2 GHz, 3.5 GHz and 3.8 GHz. It can be seen that the measured radiation patterns remain unidirectional and stable across the whole operation bands, which are in good agreement with the simulated ones. Besides, the measured HPBWs of the antenna array is 65.7 ± 4.8° and 17.5 ± 1.7° in H-plane and V-plane, separately. Excellent radiating performances make it a promising candidate for 5 G array applications.

A comparison between the proposed antenna and the reference antennas is shown in Table 1. It can be seen that our work

TABLE 1. Comparison of the proposed antenna and reference antennas.

Ref.	Dimension (λc^3)	Freq. (GHz)	Isolation (dB)	OBGSL (dB)
[1]	1.05×1.05×0.23	1.66-2.80 (51.1%) (VSWR<1.5)	>38	None
[2]	1.02×1.02×0.23	1.66-2.73 (48.7%) (VSWR<1.5)	>34	>17
[4]	0.29×0.29×0.06 (radiator)	3.3-3.6 (8.7%) (|S11|<-10dB)	>35	None
[5]	0.92×0.92×0.06	3.17-3.77 (17.2%) (|S11|<-10dB)	>38.5	None
[15]	1.04×1.04×0.09	2.46-2.78 (12.2%) (|S11|<-15dB)	>35	~ 40 (lower band)
Pro.	0.7×0.7×0.15	3.12-3.9 (22.2%) (VSWR<1.5)	>35.2	>18.5

(Here, λc represents the free-space wavelength at center frequency. OBGSL represents the out-band gain suppression level.)

has a more compact size than the other antennas. Besides, we have a wider operation band except for [1] and [2]. But their profiles are higher. Moreover, the out-band gain-suppression level in our work is better than the others except for [15]. However, the antenna proposed in [15] has one more layer to generate an extra radiation null, and the complexity is increased. In conclusion, the proposed antenna has a compact size, a low profile, as well as a high selectivity. Excellent radiating performances make it a promising candidate for 5 G base station applications using differential signals.

IV. CONCLUSION

In this paper, a differentially-fed, wideband dual-polarized filtering antenna is proposed. The three resonant modes are generated by novel E-shaped feeding structures with shorting pins, the O/SCSIRs and the square radiation patch, respectively. Besides, the O/SCSIRs offer two extra radiation nulls. Along with the U-shaped slot, the feeding structure contribute to a good bandpass filtering response of the realized gain.Measured results show that the antenna element has a wide operation band from 3.12 GHz to 3.9 GHz for active VSWR<1.5.Besides, the out-band gain suppression level is better than 18.5 dB across the operation band, which indicates a high selectivity for the proposed antenna. A 1×4 liner array is also developed to validate our design. A wide operation band with stable radiation patterns can be observed, as well as a high selectivity of better than 17.1 dB. Finally, good radiating performances of the proposed antenna are obtained, which make it a promising candidate for 5 G Sub-6 GHz base station applications.

REFERENCES

[1] Z. Tang, J. Liu, R. Lian, Y. Li, and Y. Yin, "Wideband differentially fed dual-polarized planar antenna and its array with high common-mode suppression," *IEEE Trans. Antennas Propag.*, vol. 67, no. 1, pp. 131–139, Jan. 2019.
[2] C. F. Ding, X. Y. Zhang, Y. Zhang, Y. M. Pan, and Q. Xue, "Compact broadband dual-polarized filtering dipole antenna with high selectivity for base-station applications," *IEEE Trans. Antennas Propag.*, vol. 66, no. 11, pp. 5747–5756, Nov. 2018.
[3] Y. Cui, X. Gao, and R. Li, "A broadband differentially fed dual-polarized planar antenna," *IEEE Trans. Antennas Propag.*, vol. 65, no. 6, pp. 3231–3234, Jun. 2017.
[4] H. Huang, X. Li , and Y. Liu, "A low-profile, dual-polarized patch antenna for 5G MIMO application," *IEEE Trans. Antennas Propag.*, vol. 67, no. 2, pp. 1275–1279, Feb. 2019.
[5] L.-H. Wen, S. Gao, Q. Luo, Q. Yang, W. Hu, and Y. Yin, "A low-cost differentially driven dual-polarized patch antenna by using open-loop resonators," *IEEE Trans. Antennas Propag.*, vol. 67, no. 4, pp. 2745–2750, Apr. 2019.
[6] N.-W. Liu, L. Zhu, and W.-W. Choi, "A differential-fed microstrip patch antenna with bandwidth enhancement under operation of TM_{10} and TM_{30} modes," *IEEE Trans. Antennas Propag.*, vol. 65, no. 4, pp. 1607–1614, Apr. 2017.
[7] C.-X. Mao, S. Gao, Y. Wang, Q. Luo, and Q.-X. Chu, "A shared-aperture dual-band dual-polarized filtering-antenna-array with improved frequency response," *IEEE Trans. Antennas Propag.*, vol. 65, no. 4, pp. 1836–1844, Apr. 2017.
[8] C.-X. Mao, S. Gao, Y. Wang, F. Qin, and Q.-X. Chu, "Multimode resonator-fed dual-polarized antenna array with enhanced bandwidth and selectivity," *IEEE Trans. Antennas Propag.*, vol. 63, no. 12, pp. 5492–5499, Dec. 2015.
[9] W.-J. Wu, Y.-Z. Yin, S.-L. Zuo, Z.-Y. Zhang, and J.-J. Xie, "A new compact filter-antenna for modern wireless communication systems," *IEEE Antennas Wireless Propag. Lett.*, vol. 10, pp. 1131–1134, 2011.
[10] H. Tang, C. Tong, and J.-X. Chen, "Differential dual-polarized filtering dielectric resonator antenna," *IEEE Trans. Antennas Propag.*, vol. 66, no. 8, pp. 4298–4302, Aug. 2018.
[11] L.-H. Wen, S. Gao, Q. Luo, Z. Tang, W. Hu, Y. Yin, Y. Geng, and Z. Cheng, "A balanced feed filtering antenna with novel coupling structure for low-sidelobe radar applications," *IEEE Access*, vol. 6, pp. 77169–77178, 2018.
[12] J. Y. Jin, S. Liao, and Q. Xue, "Design of filtering-radiating patch antennas with tunable radiation nulls for high selectivity," *IEEE Trans. Antennas Propag.*, vol. 66, no. 4, pp. 2125–2130, Apr. 2018.
[13] J.-F. Li, Z. N. Chen, D.-L. Wu, G. Zhang, and Y.-J. Wu, "Dual-beam filtering patch antennas for wireless communication application," *IEEE Trans. Antennas Propag.*, vol. 66, no. 7, pp. 3730–3734, Jul. 2018.
[14] X. Y. Zhang, W. Duan, and Y.-M. Pan, "High-gain filtering patch antenna without extra circuit," *IEEE Trans. Antennas Propag.*, vol. 63, no. 12, pp. 5883–5888, Dec. 2015.
[15] W. Duan, X. Y. Zhang, Y.-M. Pan, J.-X. Xu, and Q. Xue, "Dual-polarized filtering antenna with high selectivity and low cross polarization," *IEEE Trans. Antennas Propag.*, vol. 64, no. 10, pp. 4188–4196, Oct. 2016.
[16] J.-F. Qian, F.-C. Chen, Q.-X. Chu, Q. Xue, and M. J. Lancaster, "A novel electric and magnetic gap-coupled broadband patch antenna with improved selectivity and its application in MIMO system," *IEEE Trans. Antennas Propag.*, vol. 66, no. 10, pp. 5625–5629, Oct. 2018.
[17] Y. M. Pan, P. F. Hu, K. W. Leung, and X. Y. Zhang, "Compact single-/dual-polarized filtering dielectric resonator antennas," *IEEE Trans. Antennas Propag.*, vol. 66, no. 9, pp. 4474–4484, Sep. 2018.
[18] P. F. Hu, Y. M. Pan, X. Y. Zhang, and B. J. Hu, "A compact quasi-isotropic dielectric resonator antenna with filtering response," *IEEE Trans. Antennas Propag.*, vol. 67, no. 2, pp. 1294–1299, Feb. 2019.
[19] T. L. Wu, Y. M. Pan, P. F. Hu, and S. Y. Zheng, "Design of a low profile and compact omnidirectional filtering patch antenna," *IEEE Access*, vol. 5, pp. 1083–1089, 2017.
[20] B. Zhang and Q. Xue, "Filtering antenna with high selectivity using multiple coupling paths from source/load to resonators," *IEEE Trans. Antennas Propag.*, vol. 66, no. 8, pp. 4320–4325, Aug. 2018.

YAPENG LI received the B.S. degree from Xidian University, Xi'an, China, in 2012, and the M.S. degree from Lanzhou Jiaotong University, in 2016. He is currently pursuing the Ph.D. degree in electromagnetic field and microwave technology with the National Key Laboratory of Antennas and Microwave Technology, Xidian University.

His research interests include filtering antenna, wideband antenna, and circular polarized antenna.

ZHIPENG ZHAO received the B.S. degree from Xidian University, Xi'an, China, in 2015. He is currently pursuing the Ph.D. degree in electromagnetic field and microwave technology with the National Key Laboratory of Antennas and Microwave Technology, Xidian University.

His research interests include circular polarized antenna, wideband antenna, series-fed microstrip antenna array, and filtering antenna.

ZHAOYANG TANG received the B.S. and M.S. degrees from Xidian University, Xi'an, China, in 2013 and 2016, respectively. He is currently pursuing the Ph.D. degree in electromagnetic field and microwave technology with the National Key Laboratory of Antennas and Microwave Technology, Xidian University.

His research interests include multiband antennas, ultrawideband antennas, and antennas for base stations.

YINGZENG YIN received the B.S., M.S., and Ph.D. degrees in electromagnetic wave and microwave technology from Xidian University, Xi'an, China, in 1987, 1990, and 2002, respectively.

From 1990 to 1992, he was a Research Assistant and an Instructor with the Institute of Antennas and Electromagnetic Scattering, Xidian University, where he was an Associate Professor with the Department of Electromagnetic Engineering, from 1992 to 1996. Since 2004, he has been a Professor with Xidian University. His current research interests include the design of microstrip antennas, feeds for parabolic reflectors, artificial magnetic conductors, phased array antennas, base-station antennas, and computer aided design for antennas.